New Phytologist

Research

Influence of vapour pressure deficit and CO_2 on the thermal sensitivity of stomatal function in tropical trees

Alexander W. Cheesman[1], Peter Cox[2], Simon Jones[2], Kali B. Middleby[3], Lucas A. Cernusak[1] and Peter J. Franks[4]

[1]College of Science and Engineering, James Cook University, Cairns, Qld, 4878, Australia; [2]Department of Mathematics and Statistics, Faculty of Environment, Science and Economy, University of Exeter, Laver Building, North Park Road, Exeter, EX4 4QE, UK; [3]AMAP, University of Montpellier, CIRAD, CNRS, INRAE, IRD, 34398, Montpellier, France; [4]School of Life and Environmental Sciences, The University of Sydney, Sydney, NSW, 2006, Australia

Author for correspondence:
Alexander W. Cheesman
Email: alexander.cheesman@gmail.com

Received: *29 October 2025*
Accepted: *19 April 2026*

New Phytologist (2026) **251:** 1075–1087
doi: 10.1111/nph.71249

Key words: climate change, gas exchange, leaf temperature, stomatal conductance, water use.

Summary

- Stomatal conductance to water vapour (g_s) is typically considered to operate in coordination with photosynthesis (A) to balance carbon gain and water loss in an optimal manner. However, at high temperatures that suppress A, g_s has been seen to increase or remain high – reducing the predictive accuracy of some stomatal conductance models.
- We investigated the temperature sensitivity of leaf-level gas exchange and evaluated a temperature-dependent modification of a widely used stomatal conductance model across a temperature gradient (30 to 40°C) in three tropical tree species (*Mallotus philippensis*, *Ficus congesta* and *Elaeocarpus grandis*) grown and measured under near-ambient (420 ppm) or elevated (820 ppm) CO_2, and under either constant or increasing vapour pressure deficit (VPD).
- Measured A and g_s, as well as the model term g_1, all exhibited a temperature sensitivity that was impacted by [CO_2] and VPD regime. Importantly, under both constant and increasing VPD, g_1 increased with leaf temperature.
- These findings demonstrate that the coupling between A and g_s is not static but varies with temperature and environmental context, and that incorporating a representation of this thermal sensitivity provides a tractable improvement to models of plant carbon–water exchange under future climate conditions.

Introduction

In terrestrial plants, stomatal pores represent the dynamic interface of carbon and water fluxes between the leaf and the atmosphere (Berry *et al.*, 2010). As such, understanding and modelling how stomatal behaviour will be impacted by a rapidly changing climate is fundamental to predicting changes in terrestrial productivity and water use (Cox *et al.*, 1999; Damour *et al.*, 2010; Buckley & Mott, 2013; Rogers *et al.*, 2017). Generally, stomata have evolved to be highly responsive to a range of environmental cues (Clark *et al.*, 2022), including plant water status (Buckley, 2019), light intensity and quality (Vialet-Chabrand *et al.*, 2021), atmospheric CO_2 concentration (Xu *et al.*, 2016), leaf temperature (Pankasem *et al.*, 2024) and humidity – or more directly vapour pressure deficit (VPD; Grossiord *et al.*, 2020). Attempts to capture and simulate their dynamic nature have resulted in a plethora of stomatal models (Damour *et al.*, 2010). However, the prevailing theory of stomatal function in higher plants is that their responsiveness has evolved to minimise the integrated sum of $E - \lambda A$, where E is transpiration rate (mol H_2O m^{-2} s^{-1}), A is CO_2 assimilation rate (μmol CO_2 m^{-2} s^{-1}), and λ (mol H_2O mol^{-1} CO_2) represents the Lagrangian multiplier or marginal water cost of plant carbon gain (Cowan & Farquhar, 1977).

This stomatal optimisation theory has been widely explored (Buckley *et al.*, 2017), but its mathematical complexity presents practical limitations, requiring either simplifying assumptions or novel computational methods (Jones *et al.*, 2022; Potkay *et al.*, 2025a). The Medlyn *et al.* (2011) model was an attempt to reconcile the complexities of optimisation theory with the utility of empirical stomatal conductance models, such as those of Ball *et al.* (1987) and Leuning (1995), formulating stomatal conductance to water vapour (g_s, mol H_2O m^{-2} s^{-1}) as per Eqn 1:

$$g_s \approx g_0 + 1.6\left(1 + \frac{g_1}{\sqrt{VPD_L}}\right)\frac{A}{C_a} \quad \text{Eqn 1}$$

where VPD_L is vapour pressure deficit of the leaf relative to the air (kPa), C_a is the external CO_2 concentration (μmol mol^{-1}), g_0 (mol H_2O m^{-2} s^{-1}) is water loss in the absence of photosynthesis, and g_1 ($kPa^{0.5}$) is a parameter that characterises the nature of the relationship between g_s and A. The parameter g_1 reflects both

physiological and hydraulic constraints on stomatal regulation and, when calibrated for different species, encapsulates interspecific variation in water-use strategies (Buckley, 2019).

Models such as Eqn 1, which imply a coupling between A and g_s such that $\frac{dg_s}{dA}$ is always positive, have successfully explained stomatal behaviour across diverse plant types and environmental conditions (Lin *et al.*, 2015). Their simplicity and predictive capability have led to their widespread integration within the land component of Earth System Models (Lawrence *et al.*, 2019; Oliver *et al.*, 2022) and dynamic vegetation demography models (Li *et al.*, 2022). However, empirical evidence suggests that this predictable relationship becomes less reliable under high temperatures. Specifically, it has been observed that while A decreases above a thermal optimum (T_{opt}) due to the thermal sensitivity of component biochemical processes (Lin *et al.*, 2012), g_s may continue to rise (Urban *et al.*, 2017; Huang *et al.*, 2021; Feng *et al.*, 2023; Marchin *et al.*, 2023; Diao *et al.*, 2024). Such thermal 'decoupling' likely reflects a direct stomatal response to temperature (Mott & Peak, 2010; Mills *et al.*, 2024; Pankasem *et al.*, 2024) even though increasing VPD – which typically covaries with temperature – would be expected to reduce g_s (Slot *et al.*, 2024). Although empirical modifications of coupled photosynthesis-stomatal conductance models have been proposed to improve predictions under such conditions (Lamour *et al.*, 2022), these modifications tend to reduce mechanistic clarity and limit applicability under novel scenarios – a critical consideration for the utility of such models in robust climate-change projections.

Within the Medlyn *et al.* (2011) framework, the parameter g_1 is predicted to vary systematically with water-use efficiency (WUE) and plant functional type (Lin *et al.*, 2015; Miner *et al.*, 2017; Franks *et al.*, 2018). However, although commonly derived and applied as a fixed factor, g_1 is also likely to be impacted by local environmental conditions (Stefanski *et al.*, 2023; Potkay *et al.*, 2025b). In Medlyn *et al.*'s (2011) formulation, the term g_1 (Eqn 2) is considered equal to the square root of a term containing the CO_2 compensation point of A in the absence of day respiration (Γ^*, Pa) pressure (P, Pa), and the marginal water cost of carbon gain (λ, mol H_2O mol^{-1} CO_2).

$$g_1 \approx \sqrt{\frac{3\Gamma^* P\lambda}{1.6}} \qquad \text{Eqn 2}$$

Due to differences in the temperature sensitivity of CO_2 fixation and photorespiration by the photosynthetic enzyme RuBiSCO, we know that Γ^* varies substantially over a biologically relevant temperature range. This temperature dependence (Supporting Information Fig. S1) is generally assumed to be similar for all C_3 species (Bernacchi *et al.*, 2001) and can be modelled by Eqn 3 as per Sharkey *et al.* (2007),

$$\Gamma^*_T = e^{\left(c - \frac{\Delta H_a}{RT}\right)} \qquad \text{Eqn 3}$$

where c (11.187) is a scaling constant to result in a Γ^* at 25°C $\left(\Gamma^*_{25}\right)$ of 3.743 Pa, ΔH_a is enthalpy of activation (24.46 kJ mol^{-1}), and we assume $R = 8.314$ J mol^{-1} K^{-1} and temperature (T) is expressed in kelvin where (0°C = 273.15 K).

Furthermore, in their original formulation of the optimal stomatal theory, Cowan & Farquhar (1977) explicitly recognised that λ was unlikely to remain constant and would be impacted by the biophysical context of the studied plant. This dynamic view (Cowan, 1978) has often been superseded by the assumption that variation in λ arises primarily from (a) fixed species-level differences in stomatal behaviour and (b) longer-term responses to factors, such as low soil moisture availability (Manzoni *et al.*, 2011; Lin *et al.*, 2015). Nonetheless, short-term variation in λ may also arise due to temperature-driven changes in either the physical properties of water and therefore changes to the cost of water movement through the Soil–Plant–Atmosphere Continuum (SPAC) or through additional temperature dependencies of carbon gain.

For example, the viscosity (η, Pa·s) of water (inverse of fluidity) can be assumed to be independent of pressure at the earth surface but does vary with temperature over a biologically relevant range (Roderick & Berry, 2001) with viscosity at a given temperature (η_T) given by Eqn 4 (Fig. S1):

$$\eta_T = \frac{1.95 \times 10^{14}}{T_w^7} \qquad \text{Eqn 4}$$

where T_w is the temperature of the liquid water in K. This means that, as temperature increases, water becomes less viscous – that is more fluid – thereby increasing hydraulic conductance and reducing the hydraulic pressure gradient from roots to leaves for a given transpiration-driven flow rate through the xylem. This reduced viscosity of xylem sap essentially reduces the depression in leaf water potential resulting from transpiration and, with leaves maintaining higher hydration, stomata potentially maintain higher λ – that is, they will allow more water loss from leaves per unit carbon gained from photosynthesis. Note that λ here refers to the marginal water cost $\frac{dE}{dA}$ following Cowan & Farquhar (1977), in contrast to formulations like Prentice *et al.* (2014) where λ is defined as $\frac{dA}{dE}$.

At the same time, the solubility of CO_2 in the aqueous phase ($CO_{2(aq)}$) is known to be temperature-dependant, with Henry's Law coefficient at a given temperature (H^s_T, mol m^{-3} Pa^{-1}) varying across a biologically relevant range as per Eqn 5:

$$H^s_T = H^s_{25} \times e\left(B\left(\frac{1}{T_w} - \frac{1}{298.15}\right)\right) \qquad \text{Eqn 5}$$

where H^s_{25} is 0.00034 mol m^{-3} Pa^{-1}, and B is 2300 for CO_2 in fresh water (Sander, 2023).

This means that as temperature increases, the solubility of CO_2 in water decreases (Fig. S1). Given stomata respond to the substomatal CO_2 concentrations (C_i) via carbonic anhydrase enzymes functioning in stomatal guard cells (Hu *et al.*, 2010; Engineer *et al.*, 2016), a lower CO_2 solubility means that higher C_i is required to maintain the same $CO_{2(aq)}$, and this necessitates an increase in g_s, which in turn leads to higher values of λ and g_1.

If we assume a standard thermal sensitivity of Γ^* and postulate that λ changes proportionally with the inverse of change in water viscosity and the solubility of CO_2, we can expect a significant impact of temperature on theoretical g_1 (Fig. 1). Assuming all three processes contribute to an observed thermal sensitivity, this increase in g_1 would be as much as 50% between 30 and 40°C (Fig. 1). Incorporating this thermal sensitivity into predicted stomatal behaviour offers a mechanistic basis for the observed behaviour of A and g_s under elevated temperatures, wherein g_s is often found to be underestimated at higher temperatures when assuming a constant g_1 (Marchin *et al.*, 2023). Doing so could also provide a simple pathway to improve the predictive accuracy of terrestrial biosphere models employing a coupled A and g_s framework, such as the Medlyn *et al.* (2011) model, under elevated temperature (Rogers *et al.*, 2017).

In this study, we sought to develop a cohesive data set that would allow us to test the coupling between A and g_s across a range of elevated leaf temperature (T_L) and investigate how this relationship is impacted by both VPD and CO_2 concentrations [CO_2]. Specifically, we examined leaf-level gas exchange in three tropical tree species grown under low-VPD conditions and either near-ambient control (i.e. 420 ppm) or elevated (i.e. 820 ppm) CO_2. Leaf-level gas exchange was then determined with VPD_L either held constant (*c.* 1.6 kPa) or allowed to rise in line with air temperature by maintaining a constant dew point of the air. We subsequently examined whether incorporating the postulated thermal sensitivity of g_1 into the Medlyn *et al.* (2011) model could allow it to more accurately capture the observed response of g_s.

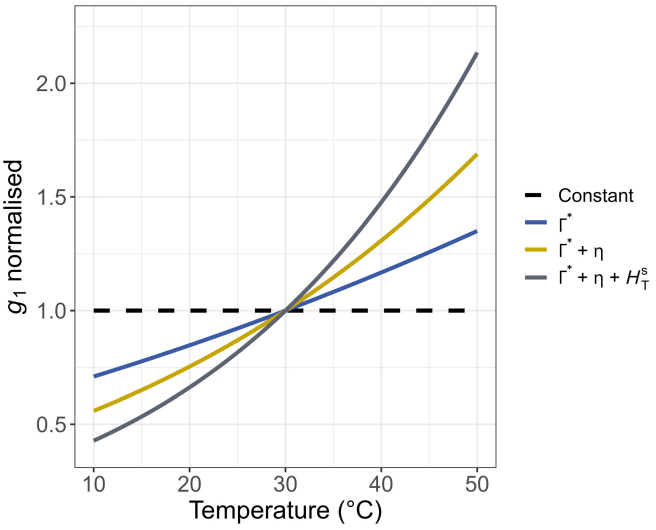

Fig. 1 Examining the potential thermal sensitivity of the model parameter g_1 when accounting for the additive nature of underlying components, including CO_2 compensation point (Γ^*) and the marginal water cost of plant carbon gain (λ), when assuming λ is dependent upon changes in the viscosity (inverse of fluidity) of water (η, Pa·s) and the solubility of CO_2 (H_T^s, mol m^{-3} Pa^{-1}). Data normalised for g_1 at 30°C using Eqn 8.

Materials and Methods

Study species and experimental material

We examined stomatal behaviour in three broadly distributed tropical tree species found within the Australian Wet Tropics: *Mallotus philippensis* (Lam.) Mull.Arg. (Euphorbiaceae), *Ficus congesta* Roxb. var. *congesta* (Moraceae) and *Elaeocarpus grandis* F.Muell. (Elaeocarpaceae; Fig. S2). All plant material was obtained from a local nursery, and for each species, the material originated from a single seed source in the lowlands. All three species show a broad geographical distribution and are typically found within the Australian Wet Tropics between sea level and 1100 m.

Seedlings were potted into 145-mm square pots (4 l) containing a high organic matter potting mix with ¼ (by volume) of a local volcanic stone, Quincan (Northside Raw Materials & Timber Supplies, Cairns, Australia), to improve drainage. Before treatments, seedlings were established in a shade house (75% solar transmission) for 1 month. At the start of the experiment, six plants per species were placed into one of two glasshouse chambers (each 2.8 × 5 m) at James Cook University's Environmental Research Complex (https://www.jcu.edu.au/environmental-research-complex). The chambers are conditioned by individual air handling units and controlled by a building management system able to provide independent control of temperature, CO_2 concentration and humidity (Middleby *et al.*, 2024).

Both chambers tracked external air temperatures, and had ultrasonic humidifiers set to turn on if VPD of the air (VPD_a) rose above 1.5 kPa. The two chambers differed in the target CO_2 concentration, set to be either a near-ambient control (420 ppm) or elevated (i.e. 820 ppm). Each chamber was fitted with a combined temperature/ relative humidity probe (HMP60; Vaisala, Vantaa, Finland) and data logger (CR300; Campbell Scientific, Logan, UT, USA) to monitor conditions independently of the building management system. To avoid unintended bias between and within chambers, pots were periodically rotated within chambers and treatments rotated between chambers every *c.* 2 months over the 6-month growing period (Fig. S3).

Gas-exchange equipment

Leaf-level gas-exchange measurements were conducted in a third climate-controlled chamber using one of three LI-6400/XT portable photosynthesis systems (LI-COR Inc., Lincoln, NE, USA) equipped with a 2 × 3 cm leaf cuvette with a red-blue LED light source (6400-02B; LI-COR). Given the inability of standard LI-6400/XT's environmental controls to provide continuous and stable humidity and CO_2 control, we pretreated inlet air to the LI-6400/XTs and bypassed the local sodalime and drierite scrubbers. Specifically, inlet air to the LI-6400/XT machines was first scrubbed of CO_2 with an external soda lime cartridge (*c.* 2 l) and pump, and then passed through one of three dew point generators (LI610; LI-COR Inc.) before being delivered at excess to T-junctions from which the LI-6400/XT could sample CO_2 free

air of a predetermined dew point. The CO_2 cylinder in each individual LI-6400/XTs was then used to deliver an inlet air stream with stable, user-defined CO_2 and H_2O concentrations.

The LI-6400/XTs were networked to a computer external to the growth chamber running LI6400XTerm v.3.4.2 while the dewpoint generators were controlled by independent 0–5 V control signals supplied by an Arbitrary Waveform Generator (AG1022; OWON, Helmond, the Netherlands). To avoid issues of condensation, air lines delivering conditioned air to the LI-6400/XTs were made of PTFE and the growth chamber temperature was generally set 2°C above the LI-6400/XTs cuvette setpoint. Nonetheless, care was still needed to stabilise the temperature profile of all components and so they were shielded from direct solar radiation with reflective panels.

Temperature ramping protocol

On days of data collection, three well-watered plants grown under low-VPD_a conditions and either control or elevated CO_2 concentrations were moved to the third chamber where the CO_2 concentration was matched to growth conditions. The LI-6400/XT cuvettes were then affixed to leaves initiated and matured under those treatment CO_2 concentrations with a standard block temperature of 30°C, photosynthetic photon flux density (PPFD) of 1000 µmol m^{-2} s^{-1}, and CO_2 concentration of incoming reference air at either 420 or 820 ppm depending on growth CO_2.

The dew point of incoming air was then adjusted to establish an initial VPD_L of between 1.5 and 1.8 kPa. After leaf-level gas exchange had stabilised to these initial conditions (typically *c.* 1 h), baseline gas-exchange measurements were collected in three successive logging periods (20 s logging for 3 min per period; total duration 9 min). Temperature ramping was then initiated by increasing both the glasshouse air temperature and the LI-6400/XT block temperature in 1°C increments.

During temperature ramping, one of two VPD regimes was applied: (a) a constant-VPD_L treatment, in which the dew point of inlet air was increased at each temperature step to maintain VPD_L approximately constant (mean curve-average $VPD_L = 1.6$ kPa; maximum curve $VPD_L = 2.2$ kPa); and (b) an increasing-VPD_L treatment, in which the dew point of inlet air was held constant, allowing VPD_L to rise inline with temperature, reaching *c.* 5 kPa at a T_L of 42.5°C (Fig. S4). In both cases, gas exchange was allowed to stabilise before the next incremental increase with data collected as per initial conditions every 2°C. Temperature ramping typically took 3.5 h and ran from a block temperature of 30 to 40°C resulting in T_L ranging, on average, from 32.4 to 42.5°C.

After ramping experiments, plants were returned to their growth chambers and were not worked on again for at least 3 d. Response curves were collected on all three species in plants grown and measured under both control and elevated CO_2, with a constant VPD_L. In the control CO_2 plants only, a second set of curves was also collected with the increasing-VPD_L treatment. For each species, approximately six (five to seven) high-quality curves were obtained per scenario tested.

Leaf-level functional traits

To provide species-level context for observed leaf-level gas exchange, at the conclusion of temperature ramping experiments leaf-level functional traits were determined on at least one leaf per replicate plant (i.e. minimum $n = 6$ per species, per growth CO_2). This included performing photosynthetic CO_2 response curves (A–C_i) at a cuvette temperature of 30°C to obtain estimates of the maximum rates of RuBisCO carboxylation (V_{cmax}) and the rates of electron transport at 1000 µmol PPFD m^{-2} s^{-1} (J_{1000}; Buckley & Diaz-Espejo, 2015). The A–C_i curves were analysed using the 'fitacis' function in the PLANTECOPHYS package in R (Duursma, 2015). To account for the control over block temperature instead of T_L (which differed from block temperature by up to 2°C), the fitted parameters V_{cmax} and J_{1000} were normalised to the typically reported 25°C using temperature response parameters from Kelly (2014). Leaf mass per unit area (LMA) was determined by scanning leaves for area calculations and then drying at 70°C until constant mass.

Data analysis

All statistical analyses and visualisations were performed using the R Statistical Software, v.4.5.1 (R Core Team, 2025). Logged data points for each curve and setpoint were used to determine WUE calculated as A/E. The g_1 parameter was calculated using the inversion-approach set out by Potkay *et al.* (2025b). In this approach, g_1 can be calculated directly using a rearrangement of Eqn 1 by assuming that $g_0 \approx 0$, as in Eqn 6, and g_c, the stomatal conductance to CO_2, is equal to (g_s/1.6). Given the controlled nature of the data collection protocol and stability of observed gas exchange, this approach was found to be equivalent to g_1 determined at each curve's individual setpoints via the typical regression method using the R PLANTECOPHYS package (Duursma, 2015; Fig. S5).

$$g_1 = \sqrt{VPD_L}\left(\frac{g_c C_a}{A} - 1\right) \quad \text{Eqn 6}$$

Parameters (e.g. T_L, VPD_L, A, g_s, E, WUE and g_1) were then averaged for each leaf at each cuvette setpoint before further analysis.

To examine whether plants had acclimated leaf-level functional traits to growth CO_2 concentration, we initially used Welch's two sample *t*-test (which does not assume equal variances between groups) to compare LMA, V_{cmax} and J_{1000} in leaves grown under both control and elevated CO_2.

We subsequently used Welch's two sample *t*-test to examine gas-exchange data (i.e. A, g_s, C_i/C_a, WUE and g_1) of leaves under the initial conditions (i.e. cuvette temperature 30°C) used in the ramping experiments. Given the unbalanced experimental design, *t*-tests were initially applied to gas-exchange data of plants grown under control CO_2 at the beginning of either constant or progressively increasing (hereafter referred to as increasing) VPD curves. We subsequently

examined the difference between plants grown under control and elevated CO_2 concentrations when VPD_L was to be held constant.

To assess the influence of VPD regime and CO_2 treatment on the temperature response of leaf-level gas exchange, we first normalised individual curves to the initial-rates observed when the cuvette was set to 30°C. Subsequently a generalised additive model (GAM) was fitted using the R-package MGCV (Wood, 2017) to the control CO_2 subset of data, allowing us to isolate the interaction between T_L and VPD regime (i.e. constant or increasing VPD_L). The general GAM form applied to describe A, g_s, WUE and C_i/C_a (Eqn 7):

$$y = s\left(T_L, \text{by} = \text{VPD}_{\text{regime}}\right) + \text{VPD}_{\text{regime}} + s(\text{species}, \text{bs} = 're') \quad \text{Eqn 7}$$

included a smooth term for T_L separately for each VPD regime, along with a main effect of VPD regime. As we were interested in the generalisable nature of observed trends, species identity was treated as a random effect to account for potential interspecific variation, with the model fitted using restricted maximum likelihood (REML) estimation. Subsequent analyses examined the influence of growth CO_2 using a similar GAM framework applied to the subset of data from both control and elevated CO_2 plants in which VPD_L was held constant.

When examining the potential difference in g_1 with increasing T_L across CO_2 and VPD regimes, we were interested in the absolute change in g_1 and thus did not normalise individual curve values for those observed under the initial conditions; instead, an additional 'curve identity' random factor was nested within species in the GAM.

After examining trends in relative leaf-level gas exchange and calculated g_1, we assessed whether incorporating temperature sensitivity into the g_1 term improved predictions of observed g_s across the full data set. For each data point, measured g_s was compared with two modelled estimates calculated using Eqn 1 (assuming negligible g_0), the corresponding A and C_a, and one of two values of g_1. Either (a) the initial g_1 determined for that leaf at a block temperature of 30°C ($g_{1(\text{ref})}$), or (b) a g_1 incorporating a postulated temperature sensitivity of g_1 (Eqn 8):

$$g_{1(T)} = g_{1(\text{ref})} \times \sqrt{\frac{\Gamma^*_T}{\Gamma^*_{\text{ref}}} \times \frac{\eta_{\text{ref}}}{\eta_T} \times \frac{H^s_{\text{ref}}}{H^s_T}} \quad \text{Eqn 8}$$

where $g_{1(T)}$ is the modified value of g_1 at the measured T_L, calculated as a proportional adjustment to the reference value $g_{1(\text{ref})}$ based on temperature-induced changes in Γ^*, η and H^s given by Eqns 3–5 with the reference temperature (ref) taken as T_L under the initial conditions (i.e. leaf chamber of 30°C).

Model performance was assessed using root mean square error (RMSE) and the coefficient of determination (R^2) as the square of the Pearson correlation coefficient between observed and predicted values. Residuals were calculated for both models, and a paired t-test was performed to determine whether the residuals differed significantly between the models.

Results

Acclimation of leaf-level functional traits

LMA varied between species (Table 1); however, there was no significant impact observed of growth CO_2 on LMA (Table 1, $t_{(9.21)} = -1.65$, $t_{(9.75)} = -0.07$, $t_{(7.7)} = -0.70$ in *Elaeocarpus*, *Ficus* and *Mallotus*, respectively, $P > 0.01$). Both V_{cmax} and J_{1000} were significantly, but differentially, impacted by growth CO_2 across the three species examined (Table 1). In *Elaeocarpus* and *Ficus*, V_{cmax} was significantly ($P < 0.01$) lower in plants grown under elevated CO_2 ($t_{(12.9)} = 3.30$ and $t_{(12.3)} = 3.16$ in *Elaeocaprus* and *Ficus*, respectively), whereas J_{1000} was not significantly different. By contrast, V_{cmax} in *Mallotus* was found to not differ significantly while there was a significant increase in J_{1000} in plants grown under elevated CO_2 ($t_{(13)} = -3.7$, $P < 0.001$). In all species, these changes resulted in a highly significant ($P < 0.001$) increase in the C_i transition point between the Rubisco-limited and electron transport-limited phases of photosynthesis for plants grown under elevated CO_2 ($t_{(7.8)} = -4.35$, $t_{(12.1)} = -5.68$, $t_{(12.4)} = -4.96$, in *Elaeocarpus*, *Ficus* and *Mallotus*, respectively).

Initial gas-exchange data indicated species-level differences in gas-exchange characteristics, with *Ficus* having the highest A and g_s and lowest WUE, while *Mallotus* had the lowest A, g_s and highest WUE (Table 1). Species-level average g_1 ranged from 4.8 $kPa^{0.5}$ in *Elaeocarpus* to 7.9 $kPa^{0.5}$ in *Ficus*. Within species, we found no significant differences in initial gas-exchange characteristics (before the temperature ramping) in plants grown under near-ambient control CO_2 and about to be measured under either constant or increasing VPD_L. By contrast, we found highly significant differences in initial gas-exchange characteristics of plants grown and measured under control and elevated CO_2 concentrations when measured under constant VPD_L. In both *Elaeocarpus* and *Ficus*, photosynthesis (A) was significantly ($P < 0.001$) higher in plants grown and measured under elevated CO_2 ($t_{(7.7)} = -4.37$, $t_{(6.9)} = -6.93$, respectively); by contrast, *Mallotus* showed no significant difference in A, but a significant reduction in g_s ($t_{(4.97)} = 2.82$, $P < 0.05$). As a result, within all species there was a highly significant ($P < 0.001$) increase in WUE of plants grown and measured under elevated CO_2 concentrations ($t_{(5.03)} = -6.09$, $t_{(4.26)} = -3.85$, $t_{(8.11)} = -4.92$ in *Elaeocarpus*, *Ficus* and *Mallotus*, respectively). Neither C_i/C_a nor g_1 showed any significant differences between plants grown and measured under control or elevated CO_2 (Table 1).

Impact of VPD on temperature response of leaf-level gas exchange

GAMs were used to assess the effects of leaf temperature (T_L) and VPD treatment (i.e. constant or increasing) on key physiological traits, including relative A, g_s, C_i/C_a and WUE (Fig. 2).

Relative A was well explained by the GAM, which accounted for 90.2% of the observed deviance (R^2-adj = 0.90; Fig. 2a), indicating a strong influence of both T_L and VPD regime ($P < 0.001$). Plants measured under constant VPD_L had significantly higher relative A across the temperature range than those

New Phytologist

Table 1 Leaf-level functional traits and initial gas exchange of three tropical tree species grown under low-VPD conditions and either near-ambient control (420 ppm) or elevated (820 ppm) CO_2 concentrations.

Growth [CO_2]	$V_{cmax(25)}$ (μmol CO_2 m^{-2} s^{-1})	$J_{1000(25)}$ (μmol m^{-2} s^{-1})	LMA (g m^{-2})	VPD	Photosynthesis (μmol CO_2 m^{-2} s^{-1})	Conductance (mol H_2O m^{-2} s^{-1})	C_i/C_a	Transpiration (mmol H_2O m^{-2} $s^{-1)}$	WUE (μmol CO_2 $mmol^{-1}$ H_2O)	g_1
Elaocarpus grandis										
Control	**38.4 ± 6.7**	81.7 ± 15.9	75 ± 6.2	Free	11.4 ± 1.5	0.20 ± 0.06	0.73 ± 0.04	2.9 ± 0.8	4.1 ± 0.6	4.2 ± 1.1
				Held	**10.5 ± 1.8**	0.21 ± 0.04	0.76 ± 0.03	3.1 ± 0.6	**3.5 ± 0.4**	5.0 ± 0.9
Elevated	**28.1 ± 5.3**	79.1 ± 9.6	80 ± 4.6	Held	**15.1 ± 1.5**	0.17 ± 0.04	0.78 ± 0.04	2.3 ± 0.4	**6.6 ± 1.1**	5.4 ± 1.3
Ficus congesta										
Control	**36.5 ± 3.9**	96.4 ± 13.0	82 ± 11.2	Free	13.5 ± 0.4	0.36 ± 0.03	0.81 ± 0.02	4.9 ± 0.4	2.8 ± 0.3	7.0 ± 0.9
				Held	**12.5 ± 1.6**	0.36 ± 0.08	0.82 ± 0.04	4.9 ± 1.0	**2.6 ± 0.5**	7.7 ± 1.9
Elevated	**30.4 ± 3.6**	97.7 ± 11.1	83 ± 13.2	Held	**19.5 ± 1.4**	0.34 ± 0.04	0.85 ± 0.02	4.3 ± 0.7	**4.7 ± 1.0**	9.0 ± 2.1
Mallotus philippensis										
Control	20.3 ± 3.7	**46.7 ± 8.9**	52 ± 9.3	Free	9.7 ± 2.0	0.20 ± 0.07	0.77 ± 0.05	2.9 ± 1.0	3.6 ± 0.9	5.2 ± 1.8
				Held	8.4 ± 3.4	**0.21 ± 0.07**	0.81 ± 0.02	2.8 ± 0.7	**2.9 ± 0.5**	6.5 ± 0.8
Elevated	22.0 ± 2.3	**62.4 ± 7.5**	55 ± 5.0	Held	9.2 ± 2.1	**0.11 ± 0.03**	0.81 ± 0.04	1.7 ± 0.3	**5.6 ± 1.3**	6.6 ± 2.1

Data represent stable gas exchange with cuvette temperature set to 30°C, and photosynthetic photon flux density (PPFD) = 1000 μmol m^{-2} s^{-1}. Variables in bold indicate a significant difference at $P < 0.05$ between plants grown under near-ambient and elevated CO_2 concentrations. Bold indicate a significant difference at $P < 0.05$ between plant grown under near-ambient and elevated CO_2 concentrations.

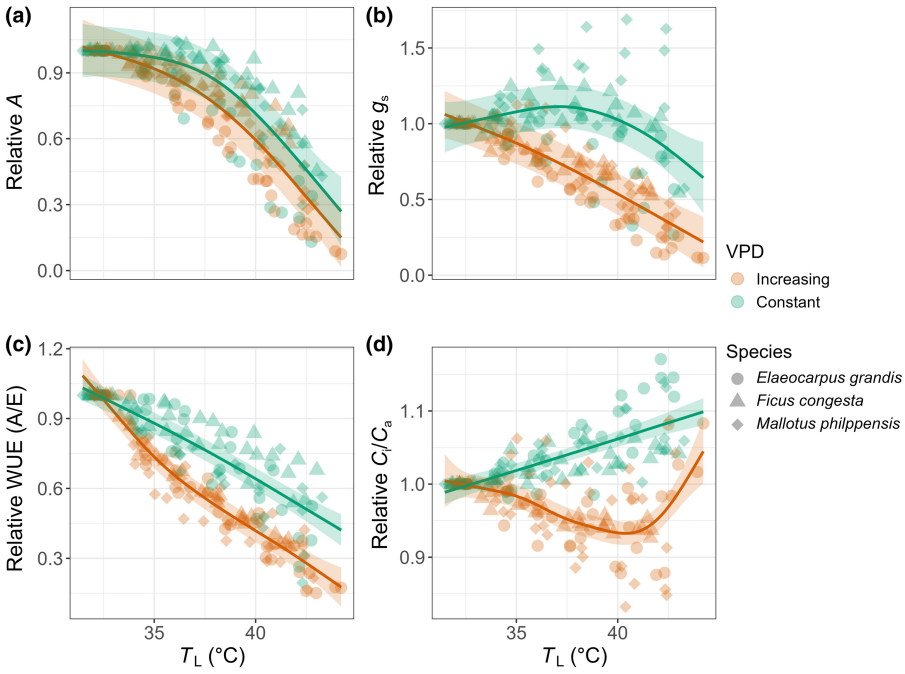

Fig. 2 Effects of leaf temperature (T_L) on relative photosynthesis (a), stomatal conductance (b), water-use efficiency (c) and C_i/C_a (d) under conditions of constant (*c.* 1.6 kPa) or progressively increasing leaf vapour pressure deficit (VPD_L) and near-ambient control (i.e. 420 ppm) CO_2. Data are shown relative to initial measurements (Table 1) with partial effects trend based on generalised additive models with species as a random factor.

under increasing VPD_L (estimated treatment effect = 0.08 ± 0.012, $P < 0.001$). While the temperature response of relative A differed significantly between VPD regimes ($P < 0.001$), with stronger thermal sensitivity and a steeper decline under increasing VPD_L (estimated degrees of freedom (edf) = 3.44, $F = 190.8$, $P < 0.001$) compared with constant VPD_L (edf = 3.60, $F = 111.0$, $P < 0.001$).

Relative g_s was also well explained by the GAM, accounting for 73.2% of the deviance (R^2-adj = 0.72, Fig. 2b). The effect of VPD regime was highly significant (estimated treatment effect = 0.31 ± 0.02, $P < 0.001$), with higher relative g_s observed under constant-VPD_L conditions. Moreover, the temperature response of relative g_s differed significantly between treatments: under increasing VPD_L, the decline in relative g_s was ostensibly linear with increasing T_L and associated VPD_L (edf = 1.77, $F = 89.2$, $P < 0.001$), whereas under constant VPD_L, relative g_s initially increased to an optimum at *c.* 38°C before a more gradual decline at very high T_L (edf = 3.10, $F = 7.62$, $P < 0.001$).

As a result of the change in A and g_s alongside changing evaporative demand under increasing VPD_L, relative WUE (i.e. A/E) exhibited a similarly strong significant ($P < 0.001$) response to both T_L and VPD regime. The GAM (R^2-adj = 0.90, deviance explained = 90%; Fig. 2c) showed plants under constant VPD_L to have significantly higher relative WUE compared with those measured under increasing VPD_L (estimated treatment effect = 0.16 ± 0.01, $P < 0.001$). The temperature response of relative

WUE was significant under both VPD regimes, with a decline observed across the temperature range in each case. Under increasing VPD_L, the decline was more pronounced (edf = 3.19, $F = 235.9$, $P < 0.001$), while under constant VPD_L, the decline was less steep but still highly significant (edf = 1.67, $F = 195.0$, $P < 0.001$).

Plants under constant VPD_L exhibited higher relative-C_i/C_a values than those under increasing VPD_L (estimate = 0.071 ± 0.005, $P < 0.001$). The temperature response of relative C_i/C_a varied significantly between treatments ($P < 0.001$), with a more complex, nonlinear temperature dependence under increasing VPD_L (edf = 4.56, $F = 9.6$, $P < 0.001$) compared with the more linear response under constant VPD_L (edf = 1.06, $F = 1.1$, $P < 0.001$). Under constant VPD_L, relative C_i/C_a generally increased with rising T_L, whereas under increasing VPD_L, it initially declined before increasing again at T_L above *c.* 41°C.

Although all species showed a similar trend with increasing T_L, species identity was found to explain a significant amount of variation in the rate of change in relative *A*, g_s and WUE across all applied models ($P < 0.001$). By contrast, the model for relative C_i/C_a (Fig. 2d; R^2-adj = 0.60, 61.4% of the deviance) revealed significant effects of T_L and VPD regime, but no significant effect of species identity.

Impact of CO_2 on temperature responses of leaf-level gas exchange

To investigate the impact of elevated CO_2 on the thermal sensitivity of relative leaf-level gas exchange under constant VPD_L, we fitted a GAM with a smooth interaction between T_L and CO_2 treatment, a main effect of CO_2 treatment and species as a random effect. The model for relative *A* explained 80% of the deviance (R^2-adj = 0.79; Fig. 3a), indicating a strong fit to the data. Plants developed and exposed to elevated CO_2 exhibited significantly higher relative *A* across the temperature range compared with those under control CO_2 (estimated treatment effect = 0.072 ± 0.015, $P < 0.001$). Temperature responses of relative *A* were significant under both CO_2 treatments, though their shapes only differed slightly (edf = 3.29 under control CO_2 and edf = 3.48 under elevated CO_2; both $P < 0.001$). The random model term species identity accounted for significant additional variation ($P < 0.001$).

The GAM for change in relative g_s explained 47.7% of the deviance (R^2-adj = 0.45; Fig. 3b), suggesting moderate predictive power. While there was no significant main effect of CO_2 treatment on relative g_s (estimated treatment effect = -0.033 ± 0.026, $P = 0.20$), the temperature responses differed significantly between CO_2 treatments. Both control and elevated CO_2 data exhibited significant temperature-dependent patterns (edf = 2.98 and 2.75, under control and elevated CO_2, respectively; both $P < 0.001$), with both showing a general increase to an optimum in relative g_s at *c.* 38°C before a decline at higher T_L. In this analysis, species identity accounted for additional significant variation (edf = 1.96, $P < 0.001$), supporting there being interspecific differences in the change in relative g_s with increasing temperature.

Relative WUE was found to generally decline with increasing T_L with the GAM explaining 61.6% of the deviance (R^2-adj = 0.60; Fig. 3c), and with a significant higher relative WUE under elevated CO_2 (estimated treatment effect = 0.077 ± 0.018, $P < 0.001$). The temperature dependence of relative WUE differed between treatments: under control CO_2, relative WUE decreased linearly with temperature (edf = 1.00, $F = 156.1$, $P < 0.001$), while under elevated CO_2 the response declined but was more complex (edf = 3.32, $F = 28.7$, $P < 0.001$), suggesting that elevated CO_2 not only enhances relative WUE but also modifies its thermal response. Species identity also accounted for significant variation (edf = 1.6, $P < 0.01$).

Relative C_i/C_a increased with increasing T_L under constant VPD_L and both control and elevated CO_2 concentrations (Fig. 3d). The relative-C_i/C_a GAM explained 44.5% of the deviance (R^2adj = 0.42) suggesting moderate predictive power. Elevated CO_2 significantly reduced relative C_i/C_a (estimated treatment effect = -0.0251 ± 0.005, $P < 0.001$), likely due to the noted higher photosynthetic demand, while the smooth term for T_L was still significant under both treatments (edf =1.36 and 3.37, under control and elevated CO_2, respectively. $P < 0.001$) showing an increase in relative C_i/C_a with increasing T_L. Species variation in relative C_i/C_a was present but less pronounced than in other parameters (edf = 1.45, $P < 0.05$).

Temperature sensitivity of g_1

We examined variation in the stomatal model parameter g_1 across experimental treatments and a range in T_L to provide insight into possible changes in stomatal coupling to photosynthesis (Fig. 4). Initially we examined the change in g_1 across increasing T_L under near-ambient control CO_2 concentrations and either constant or increasing VPD_L (Fig. 4a). The GAM explained 70.2% of the deviance (R^2-adj = 0.64). Across the data set, there was a significant main effect of VPD regime, with higher g_1 values under constant-VPD_L conditions (estimated treatment effect = 2.06 ± 0.99, $P = 0.040$). Leaf temperature was found to have a significant and nonlinear influence on g_1 under both increasing and constant VPD_L (edf = 2.75 and 2.71, respectively; both $P < 0.001$), with a stronger temperature response evident under constant VPD_L ($F = 30.16$) compared with increasing VPD_L ($F = 14.22$). The random effect of curve identity contributed significantly to model fit ($P < 0.001$), whereas the species-level effect was not significant ($P = 0.13$), suggesting variation in g_1 was more strongly associated with individual leaf context than species identity.

When examining the trends in g_1 over T_L between CO_2 treatments (Fig. 4b), the GAM explained 71.3% of the deviance (adjusted $R^2 = 0.65$). No significant main effect of CO_2 treatment was detected (estimated treatment effect = -0.73 ± 1.15, $P = 0.531$), indicating that elevated CO_2 did not alter the overall magnitude of g_1. However, the shape of the temperature response of g_1 differed significantly between treatments. The smooth functions describing the relationship between T_L and g_1 were significant under both control and elevated CO_2 (edf = 2.60 and 2.79, respectively; both $P < 0.001$), indicating strong nonlinear temperature responses, but the temperature response was more

New Phytologist

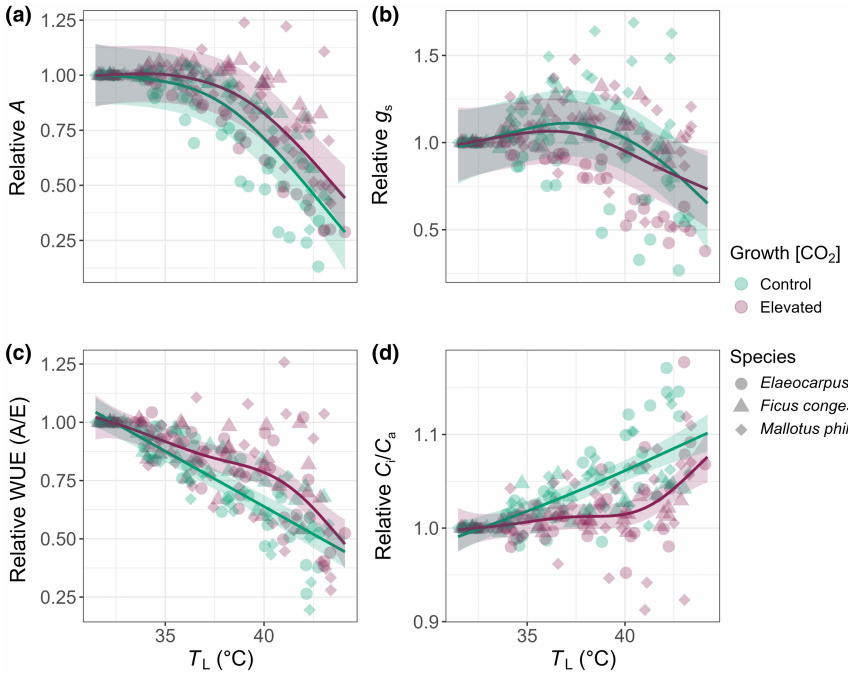

Fig. 3 Effects of leaf temperature (T_L) on relative photosynthesis (a), stomatal conductance (b), water-use efficiency (c) and C_i/C_a (d) of leaves under conditions of constant – vapour pressure deficit (*c*. 1.6 kPa) and either near-ambient control (i.e. 420 ppm) or elevated (820 ppm) CO_2 reflecting long-term growth conditions of plants. Data are shown relative to initial measurements conditions (see Table 1) with partial effects trend based on generalised additive models with species as a random factor.

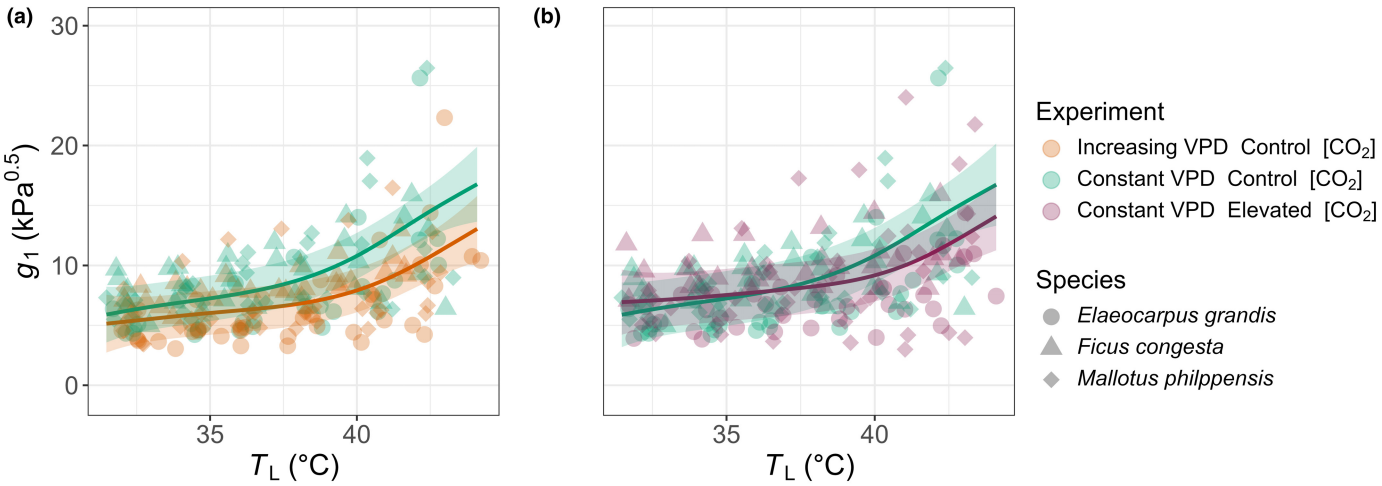

Fig. 4 Observed response of stomatal model parameter g_1 (kPa$^{0.5}$) as defined by Medlyn *et al*. (2011) to leaf temperature (T_L) under near-ambient control CO_2 and either increasing or constant vapour pressure deficit (VPD) (a), or constant low-VPD and either control or elevated CO_2 (b). Observations shown for three species of tropical tree as well as trends predicted from a generalised additive model, including random effects of species and curve identity.

pronounced under control CO_2 ($F = 27.29$) compared with elevated CO_2 ($F = 12.72$), suggesting a dampening of g_1 thermal sensitivity under elevated CO_2. The random effect of curve identity nested within species contributed significantly to model fit ($P = 0.003$), while the species-level random effect alone was not significant ($P = 0.08$).

Incorporating temperature sensitivity of g_1

We compared observed g_s with modelled values using two approaches: one using a constant g_1 determined at the initiation of each curve (Fig. 5a), and another incorporating the postulated temperature sensitivity of g_1 (Fig. 5b). The model that included temperature sensitivity performed better, with a lower RMSE (0.028 vs 0.045) and a higher coefficient of determination ($R^2 = 0.94$ vs $R^2 = 0.91$). Residual analysis confirmed a significant improvement in model fit when the temperature sensitivity of g_1 was included. A paired *t*-test comparing residuals of the two models showed a highly significant difference ($t = 17.13$, df = 295, $P < 0.001$), with the temperature-sensitive model exhibiting consistently lower residuals (mean difference = 0.027, CI = 0.024–0.030 mol m^{-2} s^{-1}).

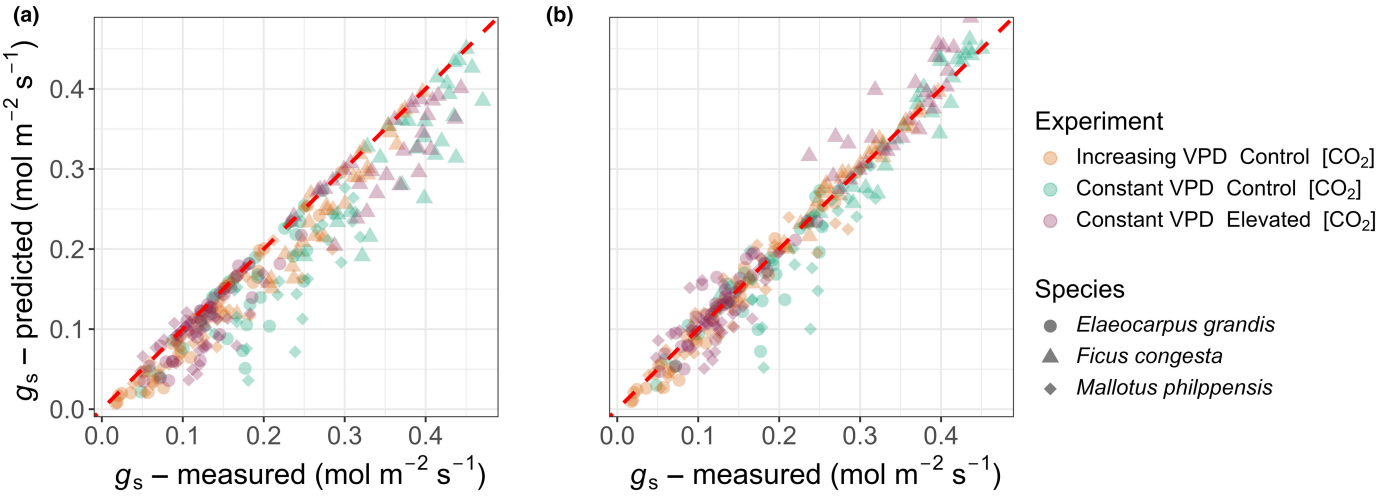

Fig. 5 Comparison between measured g_s and g_s predicted using (a) constant g_1 based on the initial data for each curve or (b) the initial g_1 modified to account for postulated temperature sensitivity. Dashed red line indicates 1 : 1.

Discussion

Understanding how stomatal behaviour responds to rising temperatures is essential for predicting plant carbon–water dynamics under future climates (Blonder *et al.*, 2023). Here, we sought to assess how variation in leaf temperature (T_L), CO_2 concentration and temperature-VPD regime (i.e. whether VPD_L was constrained or covaried with T_L) influences the coupling between photosynthesis (A) and stomatal conductance (g_s) in well-watered saplings of three diverse tropical tree species. Our results demonstrate that both VPD regime and CO_2 can significantly modify the observed thermal responses of A, g_s, WUE and the stomatal model parameter g_1. Critically, we also show that incorporating a mechanistically derived temperature-sensitive formulation of the model parameter g_1 improves the predictive accuracy of the Medlyn *et al.* (2011) model at high temperatures.

Elevated CO_2 alters photosynthetic capacity but not intrinsic stomatal regulation

Growth under elevated CO_2 induced species-specific adjustments in photosynthetic capacity, but without coordinated changes in leaf structural traits (i.e. LMA) or intrinsic stomatal behaviour. In *Elaeocarpus* and *Ficus*, elevated CO_2 reduced V_{cmax} without altering J_{1000}, whereas *Mallotus* apparently maintained V_{cmax} but exhibited enhanced electron transport capacity. Despite these contrasting biochemical responses, all species showed an increase in the C_i transition point and a consistent enhancement of WUE under elevated CO_2 typical of plants grown under elevated CO_2 (Cernusak *et al.*, 2019; Ainsworth & Long, 2021). Neither C_i/C_a nor g_1 differed between growth CO_2 treatments, indicating that elevated CO_2 did not alter intrinsic stomatal regulation, consistent with Gardner *et al.* (2023). Observed g_1 under initial conditions (i.e. Li6400/XT cuvette at 30°C), across the three species averaged 6.3 $kPa^{0.5}$ (range 4.9 to 7.9 $kPa^{0.5}$). This is substantially larger than that originally reported for rainforest trees by Lin *et al.* (2015; i.e. 3.77 $kPa^{0.5}$) but which is comparable to the value used by more recent analysis by Oliver *et al.* (2022) when calibrating the land surface model JULES vn 5.6 (i.e. 5.31 $kPa^{0.5}$).

VPD shapes the thermal responses of leaf-level gas exchange

In this study, measurements of plants under contrasting VPD regimes (i.e. constant or increasing) demonstrated that evaporative demand strongly shapes the temperature responses of leaf-level gas exchange in tropical plants grown under near-ambient CO_2. When VPD_L was allowed to rise with increasing T_L, both relative A and relative g_s were lower than values measured at comparable T_L made under constant (and low) VPD_L (Fig. 2). These responses are consistent with previous work showing that high VPD_L suppresses g_s and can lower the temperature at which rates of A begin to decline (Grossiord *et al.*, 2020; Slot *et al.*, 2024). Indeed, the two VPD regimes clearly diverged in how g_s constrained C_i (and thereby A). Under constant-VPD_L, g_s did not immediately decline with increasing T_L and initially continued to rise, resulting in an increase in C_i/C_a despite declining A at higher temperatures. By contrast, when VPD_L increased with T_L, g_s declined progressively, reducing C_i/C_a and imposing a stomatal limitation on photosynthesis. Only at very high temperatures ($T_L > 41$°C), where A had declined to very low rates, did C_i/C_a increase again under rising VPD_L, reflecting the collapse of biochemical demand for CO_2 rather than stomatal reopening. WUE declined under both VPD regimes, though more rapidly under increasing VPD_L, underscoring that changes in transpiration across T_L reflect both stomatal regulation and the direct influence of VPD_L on evaporative flux.

Our results indicate that VPD_L modulates the apparent thermal sensitivity of g_1, with a stronger temperature dependence observed when VPD_L was held constant (Fig. 4a). At face value, this might suggest that the impact of VPD_L on g_s is incompletely captured by the inverse, square root term in Eqn 1. However, caution is warranted in interpreting this pattern. The calculation

of g_s from leaf-level gas-exchange data assumes that the air within the substomatal cavity is fully saturated with water vapour. In reality, this assumption can fail to be met, especially in leaves being measured under high VPD_L (Cernusak *et al.*, 2024). When leaves are unable to maintain saturation of the internal air space, g_s may be underestimated as a result of additional 'unsaturation resistance' to water movement being wrongly assigned to stomatal resistance (Wong *et al.*, 2022). When the potential impact of unsaturation on calculated g_s has been examined in detail, it has been found to be as much as 30% under moderate-to-high VPD_L (Wong *et al.*, 2022; Cernusak *et al.*, 2024). It is therefore possible that the observed difference in g_1 and C_i/C_a as a result of increasing-VPD treatment (Fig. 4a) reflects, at least in part, the influence of substomatal unsaturation leading to an increasing underestimation of g_s as VPD_L increases.

Impacts of elevated CO_2 on stomatal behaviour

Measurement of leaf-level gas exchange under elevated CO_2 demonstrated substantial acclimation in leaf function (Table 1). While all three species saw an increase in the C_i transition point between RuBP carboxylation and RuBP regeneration limitation, *Ficus* and *Elaeocarpus* achieved this through a reduction in V_{cmax}, while *Mallotus* showed no change in V_{cmax} but rather an increase in J_{1000}. All species saw a significant increase in WUE – consistent with the well-established CO_2 fertilisation effect (Cernusak *et al.*, 2019). In two of the species (*Ficus* and *Elaeocarpus*), this was predominantly due to an increase in A, while in *Mallotus* it was due to a reduction in g_s. This difference may reflect a difference in the species' ecological niche, with *Mallotus* being typically found in monsoonal and drier rainforest where water availability is often a limiting factor, possibly favouring selection for more conservative water use (Zich *et al.*, 2020).

Across all three species, there was no significant change observed in g_1 across growth CO_2 (Table 1), suggesting that the coordination between photosynthetic capacity and stomatal function is at least partially maintained under elevated CO_2 (Fig. 3; Gardner *et al.*, 2023). However, we did observe significant shifts in the temperature sensitivity of relative gas exchange under elevated CO_2 (Figs 3, 4b). Although our data do not include T_L low enough to allow for the reliable determination of T_{opt} (i.e. thermal optimum for A), the apparent increase in T_{opt} (Fig. 3a) under elevated CO_2 is consistent with the known direct modification of photosynthetic biochemistry under elevated CO_2 (Long, 1991; Smith & Keenan, 2020) as well as the coordinated acclimation of stomatal and mesophyll function (Hu *et al.*, 2026). It is this increase in T_{opt} and therefore the rate and shape of temperature-induced decline in A that may directly impact the observed difference in temperature response of g_1 under elevated CO_2.

Incorporating temperature sensitivity into stomatal models

The theoretical foundation of coupled photosynthesis-stomata models such as Medlyn *et al.* (2011) suggests that g_1 scales with both the CO_2 compensation point (Γ^*) and the marginal water cost of carbon gain (λ), both of which are likely temperature-sensitive (Sharkey *et al.*, 2007; Prentice *et al.*, 2014). By explicitly incorporating temperature dependencies of Γ^*, water viscosity (η) and solubility of CO_2 in water (H^s) into a predictive framework for g_1, we were able to mechanistically estimate how stomatal sensitivity should change with T_L (Fig. 1). Incorporating this dynamic temperature-sensitive g_1 into the Medlyn *et al.* (2011) model resulted in model behaviour that qualitatively matched that observed within our data set, including the relative trends in A, g_s and C_i/C_a with increasing temperature, and under both elevated CO_2 and different VPD treatments (See Data availability statement and Figs S6–S8). Moreover, using this temperature-sensitive g_1 significantly improved predictions of g_s at elevated temperatures reducing RMSE by 37% across our diverse leaf-level gas-exchange data (Fig. 5).

While previous studies have adjusted g_1 empirically to improve model fit under heat stress (Lamour *et al.*, 2022), it is clear that there exists a temperature dependence in the stomatal relationship to photosynthesis in at least well-watered C_3 plants (Pankasem *et al.*, 2024; Chen *et al.*, 2025). Reanalysis of previously published data on stomatal 'decoupling' in temperate tree species by Diao *et al.* (2024) provides further evidence for this (Fig. S9). By applying Potkay *et al.*'s (2025b) inversion method to examine g_1, it is clear that there is highly significant temperature sensitivity of g_1 under constant VPD_L, between 5 and 35°C in the three angiosperms *Fagus sylvatica*, *Quercus petraea* and *Tilia cordata* – although not in the gymnosperm *Picea abies*, that also had a lower g_1. In the angiosperms which showed a temperature sensitivity – values rose from a minimum observed g_1 at *c.* 20 to 25°C corresponding with an apparent minimum in C_i/C_a (Diao *et al.*, 2024). At very low temperatures (i.e. 5°C) g_1 was also found to be higher; however, it is unclear whether this represents a true change in the coupling between g_s and A, or an artefact that arises due to changes in the signal to noise ratio at very low rates of A and g_s (Fig. S9).

Decoupled but mechanistically linked

Our results (Fig. 2b), together with those of Diao *et al.* (2024) and in Mills *et al.* (2024), demonstrate that under constant evaporative demand, g_s does not always increase monotonically with T_L. Instead, g_s may stabilise or decline at high T_L. This behaviour results from g_s being simultaneously responsive to multiple, potentially antagonistic, environmental cues. At very high T_L, biochemical limitations constrain A resulting in a response in g_s via an increase in C_i that may counter any direct temperature stomatal response (Mills *et al.*, 2024; Takahashi *et al.*, 2025). Furthermore, our incorporation of a temperature-sensitive g_1 term within the Medlyn *et al.* (2011) model shows that, within a coupled framework, g_s may still increase under conditions where A declines. Similar outcomes also arise in optimisation-based models that incorporate the benefits of transpirational cooling at high temperatures (Friend, 1995; Sabot *et al.*, 2022). This is consistent with strong selective pressures favouring elevated g_s to mitigate thermal stress during temperature extremes (Drake *et al.*, 2018). In this context, it should be noted that, even when $\frac{dg_s}{dA} < 0$, A and g_s may remain mechanistically linked.

Other sources of temperature sensitivity

An often-implicit assumption when employing stomatal models such as Medlyn *et al.* (2011) is that water loss in the absence of photosynthesis is minimal and can be discounted when considering changes in leaf-level gas exchange in illuminated leaves (i.e. $g_0 \approx 0$). This leads to the prediction that when A declines to zero due to thermal constraints g_s also tends to zero (Fig. S6). However, minimum conductance (g_{min}) due to incomplete stomatal closure or cuticular leakiness, while typically low, is not zero (Duursma *et al.*, 2019). Moreover, emerging evidence suggests a thermal sensitivity in g_{min} (Slot *et al.*, 2021) and that this behaviour occurs through multiple physiological pathways (Garen & Michaletz, 2025). While Slot *et al.* (2021) showed minimal change in g_{min} of tropical tree species between 30 and 40°C, in situations where measured water loss declines substantially, g_{min} and its thermal sensitivity may play a more prominent role – leading to a breakdown in the assumption that g_0 is negligible. Incorporating temperature-dependent formulations of g_{min}, or its mathematical operator equivalent g_0, could therefore improve stomatal models, particularly under supra-optimal thermal or VPD stress where this residual conductance could play a larger proportional role in overall water loss.

Conclusion and outlook

Most vegetation models that employ a photosynthesis-conductance coupled formulation, such as Medlyn *et al.* (2011) apply static values for parameters like g_1 (Bonan *et al.*, 2014; Oliver *et al.*, 2022). However, our results, together with emerging evidence from other systems (Chen *et al.*, 2025), demonstrate that the coupling between A and g_s in well-watered plants is dynamically modulated by temperature and growth environment. In our data, incorporating a generalised thermal sensitivity of g_1 improved predictions of g_s across all experimental treatments tested here, with the largest gains in accuracy occurring at supra-optimal temperatures for photosynthesis where models assuming a constant g_1 systematically underestimate g_s.

Importantly, the value of this approach is expected to be greatest when extrapolating stomatal behaviour beyond the temperature range over which g_1 has been parameterised, such as under future climate scenarios – characterised by more frequent and intense temperature extremes. While the formulation presented here does not yet account for second-order interactions and possible shifts in the thermal sensitivity of g_1 with VPD regime or CO_2 concentration, it offers a mechanistically grounded and computationally tractable pathway for improving projections of plant water use and carbon–water coupling in Earth system and vegetation models operating under projected future climate change.

Acknowledgements

We acknowledge funding for this research from the Human Frontier Science Program RGP0016/2020 awarded to PJF and PC, and from the Australian Research Council by way of a Discovery Project DP20101938 awarded to LAC. Open access publishing facilitated by James Cook University, as part of the Wiley - James Cook University agreement via the Council of Australasian University Librarians

Competing interests

None declared.

Author contributions

AWC, LC, PJF and PC planned and designed the research. AWC and KBM performed experiments and analysed data with interpretation from all authors. AWC, LAC and KBM wrote the manuscript draft, with all authors contributing to the final edit.

ORCID

Lucas A. Cernusak https://orcid.org/0000-0002-7575-5526
Alexander W. Cheesman https://orcid.org/0000-0003-3931-5766
Peter Cox https://orcid.org/0000-0002-0679-2219
Peter J. Franks https://orcid.org/0000-0002-4810-658X
Simon Jones https://orcid.org/0000-0002-2653-2318
Kali B. Middleby https://orcid.org/0000-0002-9323-0870

Data availability

Data and code used in this manuscript are available at the Dryad Data Repository https://doi.org/10.5061/dryad.tdz08kqc9.

References

Ainsworth EA, Long SP. 2021. 30 years of free-air carbon dioxide enrichment (FACE): what have we learned about future crop productivity and its potential for adaptation? *Global Change Biology* **27**: 27–49.

Ball J, Berry J, Woodrow I. 1987. A model predicting stomatal conductance and its contribution to the control of photosynthesis under different environmental conditions. In: *Progress in photosynthesis research.* Dordrecht, the Netherlands: Martinus Nijhoff Publishers, 221–224.

Bernacchi CJ, Singsaas EL, Pimentel C, Portis AR, Long SP. 2001. Improved temperature response functions for models of Rubisco-limited photosynthesis. *Plant, Cell & Environment* **24**: 253–259.

Berry JA, Beerling DJ, Franks PJ. 2010. Stomata: key players in the earth system, past and present. *Current Opinion in Plant Biology* **13**: 233–240.

Blonder BW, Aparecido LMT, Hultine KR, Lombardozzi D, Michaletz ST, Posch BC, Slot M, Winter K. 2023. Plant water use theory should incorporate hypotheses about extreme environments, population ecology, and community ecology. *New Phytologist* **238**: 2271–2283.

Bonan GB, Williams M, Fisher RA, Oleson KW. 2014. Modeling stomatal conductance in the earth system: linking leaf water-use efficiency and water transport along the soil-plant-atmosphere continuum. *Geoscientific Model Development* **7**: 2193–2222.

Buckley TN. 2019. How do stomata respond to water status? *New Phytologist* **224**: 21–36.

Buckley TN, Diaz-Espejo A. 2015. Reporting estimates of maximum potential electron transport rate. *New Phytologist* **205**: 14–17.

Buckley TN, Mott KA. 2013. Modelling stomatal conductance in response to environmental factors. *Plant, Cell & Environment* **36**: 1691–1699.

Buckley TN, Sack L, Farquhar GD. 2017. Optimal plant water economy. *Plant, Cell & Environment* **40**: 881–896.

Cernusak LA, Haverd V, Brendel O, Le Thiec D, Guehl JM, Cuntz M. 2019. Robust response of terrestrial plants to rising CO_2. *Trends in Plant Science* **24**: 578–586.

Cernusak LA, Wong SC, Stuart-Williams H, Márquez DA, Pontarin N, Farquhar GD. 2024. Unsaturation in the air spaces of leaves and its implications. *Plant, Cell & Environment* **47**: 3685–3698.

Chen YT, Liang KH, Cui BJ, Hou JX, Rosenqvist E, Fang L, Liu FL. 2025. Incorporating the temperature responses of stomatal and non-stomatal limitations to photosynthesis improves the predictability of the unified stomatal optimization model for wheat under heat stress. *Agricultural and Forest Meteorology* **362**: 13.

Clark JW, Harris BJ, Hetherington AJ, Hurtado-Castano N, Brench RA, Casson S, Williams TA, Gray JE, Hetherington AM. 2022. The origin and evolution of stomata. *Current Biology* **32**: R539–R553.

Cowan IR. 1978. Stomatal behaviour and environment. In: Preston RD, Woolhouse HW, eds. *Advances in botanical research*. London, UK: Academic Press, 117–228.

Cowan IR, Farquhar GD. 1977. Stomatal function in relation to leaf metabolism and environment. *Symposia of the Society for Experimental Biology* **31**: 471–505.

Cox PM, Betts RA, Bunton CB, Essery RLH, Rowntree PR, Smith J. 1999. The impact of new land surface physics on the GCM simulation of climate and climate sensitivity. *Climate Dynamics* **15**: 183–203.

Damour G, Simonneau T, Cochard H, Urban L. 2010. An overview of models of stomatal conductance at the leaf level. *Plant, Cell & Environment* **33**: 1419–1438.

Diao H, Cernusak LA, Saurer M, Gessler A, Siegwolf RTW, Lehmann MM. 2024. Uncoupling of stomatal conductance and photosynthesis at high temperatures: mechanistic insights from online stable isotope techniques. *New Phytologist* **241**: 2366–2378.

Drake JE, Tjoelker MG, Vårhammar A, Medlyn BE, Reich PB, Leigh A, Pfautsch S, Blackman CJ, López R, Aspinwall MJ *et al.* 2018. Trees tolerate an extreme heatwave via sustained transpirational cooling and increased leaf thermal tolerance. *Global Change Biology* **24**: 2390–2402.

Duursma RA. 2015. Plantecophys - An R package for analysing and modelling leaf gas exchange data. *PLoS ONE* **10**: 13.

Duursma RA, Blackman CJ, Lopéz R, Martin-StPaul NK, Cochard H, Medlyn BE. 2019. On the minimum leaf conductance: its role in models of plant water use, and ecological and environmental controls. *New Phytologist* **221**: 693–705.

Engineer CB, Hashimoto-Sugimoto M, Negi J, Israelsson-Nordström M, Azoulay-Shemer T, Rappel W-J, Iba K, Schroeder JI. 2016. CO_2 sensing and CO_2 regulation of stomatal conductance: Advances and open questions. *Trends in Plant Science* **21**: 16–30.

Feng X, Liu R, Li C, Zhang H, Slot M. 2023. Contrasting responses of two C4 desert shrubs to drought but consistent decoupling of photosynthesis and stomatal conductance at high temperature. *Environmental and Experimental Botany* **209**: 105295.

Franks PJ, Bonan GB, Berry JA, Lombardozzi DL, Holbrook NM, Herold N, Oleson KW. 2018. Comparing optimal and empirical stomatal conductance models for application in Earth system models. *Global Change Biology* **24**: 5708–5723.

Friend AD. 1995. PGEN: an integrated model of leaf photosynthesis, transpiration, and conductance. *Ecological Modelling* **77**: 233–255.

Gardner A, Jiang MK, Ellsworth DS, MacKenzie AR, Pritchard J, Bader MKF, Barton CVM, Bernacchi C, Calfapietra C, Crous KY *et al.* 2023. Optimal stomatal theory predicts CO_2 responses of stomatal conductance in both gymnosperm and angiosperm trees. *New Phytologist* **237**: 1229–1241.

Garen JC, Michaletz ST. 2025. Temperature governs the relative contributions of cuticle and stomata to leaf minimum conductance. *New Phytologist* **245**: 1911–1923.

Grossiord C, Buckley TN, Cernusak LA, Novick KA, Poulter B, Siegwolf RTW, Sperry JS, McDowell NG. 2020. Plant responses to rising vapor pressure deficit. *New Phytologist* **226**: 1550–1566.

Hu H, Boisson-Dernier A, Israelsson-Nordström M, Böhmer M, Xue S, Ries A, Godoski J, Kuhn JM, Schroeder JI. 2010. Carbonic anhydrases are upstream regulators of CO_2-controlled stomatal movements in guard cells. *Nature Cell Biology* **12**: 87–93.

Hu X, Wong SC, Farquhar GD. 2026. Coordinated stomatal, mesophyll, and biochemical functions facilitate photosynthetic adaptation to heat and dryness. *Proceedings of the National Academy of Sciences, USA* **123**: e2605032123.

Huang G, Yang Y, Zhu L, Peng S, Li Y. 2021. Temperature responses of photosynthesis and stomatal conductance in rice and wheat plants. *Agricultural and Forest Meteorology* **300**: 108322.

Jones S, Eller CB, Cox PM. 2022. Application of feedback control to stomatal optimisation in a global land surface model. *Frontiers in Environmental Science* **10**: 2022.

Kelly J. 2014. *Productivity and water use of Australian tree species under climate change*. PhD thesis, NSW, Australia: Macquarie University.

Lamour J, Davidson KJ, Ely KS, Le Moguédec G, Leakey ADB, Li QY, Serbin SP, Rogers A. 2022. An improved representation of the relationship between photosynthesis and stomatal conductance leads to more stable estimation of conductance parameters and improves the goodness-of-fit across diverse data sets. *Global Change Biology* **28**: 3537–3556.

Lawrence DM, Fisher RA, Koven CD, Oleson KW, Swenson SC, Bonan G, Collier N, Ghimire B, van Kampenhout L, Kennedy D *et al.* 2019. The Community Land Model Version 5: description of new features, benchmarking, and impact of forcing uncertainty. *Journal of Advances in Modeling Earth Systems* **11**: 4245–4287.

Leuning R. 1995. A critical appraisal of a combined stomatal-photosynthesis model for C_3 plants. *Plant, Cell & Environment* **18**: 339–355.

Li Q, Serbin SP, Lamour J, Davidson KJ, Ely KS, Rogers A. 2022. Implementation and evaluation of the unified stomatal optimization approach in the Functionally Assembled Terrestrial Ecosystem Simulator (FATES). *Geoscientific Model Development* **15**: 4313–4329.

Lin Y-S, Medlyn BE, Duursma RA, Prentice IC, Wang H, Baig S, Eamus D, de Dios Victor R, Mitchell P, Ellsworth DS *et al.* 2015. Optimal stomatal behaviour around the world. *Nature Climate Change* **5**: 459–464.

Lin Y-S, Medlyn BE, Ellsworth DS. 2012. Temperature responses of leaf net photosynthesis: the role of component processes. *Tree Physiology* **32**: 219–231.

Long SP. 1991. Modification of the response of photosynthetic productivity to rising temperature by atmospheric CO_2 concentrations: Has its importance been underestimated? *Plant, Cell & Environment* **14**: 729–739.

Manzoni S, Vico G, Katul G, Fay PA, Polley W, Palmroth S, Porporato A. 2011. Optimizing stomatal conductance for maximum carbon gain under water stress: a meta-analysis across plant functional types and climates. *Functional Ecology* **25**: 456–467.

Marchin RM, Medlyn BE, Tjoelker MG, Ellsworth DS. 2023. Decoupling between stomatal conductance and photosynthesis occurs under extreme heat in broadleaf tree species regardless of water access. *Global Change Biology* **29**: 6319–6335.

Medlyn BE, Duursma RA, Eamus D, Ellsworth DS, Prentice IC, Barton CVM, Crous KY, de Angelis P, Freeman M, Wingate L. 2011. Reconciling the optimal and empirical approaches to modelling stomatal conductance. *Global Change Biology* **17**: 2134–2144.

Middleby KB, Cheesman AW, Cernusak LA. 2024. Impacts of elevated temperature and vapour pressure deficit on leaf gas exchange and plant growth across six tropical rainforest tree species. *New Phytologist* **243**: 648–661.

Mills C, Bartlett MK, Buckley TN. 2024. The poorly-explored stomatal response to temperature at constant evaporative demand. *Plant, Cell & Environment* **47**: 3428–3446.

Miner GL, Bauerle WL, Baldocchi DD. 2017. Estimating the sensitivity of stomatal conductance to photosynthesis: a review. *Plant, Cell & Environment* **40**: 1214–1238.

Mott KA, Peak D. 2010. Stomatal responses to humidity and temperature in darkness. *Plant, Cell & Environment* **33**: 1084–1090.

Oliver RJ, Mercado LM, Clark DB, Huntingford C, Taylor CM, Vidale PL, McGuire PC, Todt M, Folwell S, Shamsudheen Semeena V *et al.* 2022. Improved representation of plant physiology in the JULES-vn5.6 land surface model: photosynthesis, stomatal conductance and thermal acclimation. *Geoscientific Model Development* **15**: 5567–5592.

Pankasem N, Hsu P-K, Lopez BNK, Franks PJ, Schroeder JI. 2024. Warming triggers stomatal opening by enhancement of photosynthesis and ensuing guard cell CO_2 sensing, whereas higher temperatures induce a photosynthesis-uncoupled response. *New Phytologist* **244**: 1847–1863.

Potkay A, Cabon A, Peters RL, Fonti P, Sapes G, Sala A, Stefanski A, Butler E, Bermudez R, Montgomery R *et al.* 2025a. Generalized stomatal optimization of evolutionary fitness proxies for predicting plant gas exchange under drought, heatwaves, and elevated CO_2. *Global Change Biology* **31**: e70049.

Potkay A, Sloan B, Feng X. 2025b. Stomatal parameters in a changing environment. *Plant, Cell & Environment* **48**: 2986–2997.

Prentice IC, Dong N, Gleason SM, Maire V, Wright IJ. 2014. Balancing the costs of carbon gain and water transport: testing a new theoretical framework for plant functional ecology. *Ecology Letters* **17**: 82–91.

R Core Team. 2025. *R: a language and environmental for statistical computing.* Vienna, Austria: R Foundation for Statistical Computing.

Roderick ML, Berry SL. 2001. Linking wood density with tree growth and environment: a theoretical analysis based on the motion of water. *New Phytologist* **149**: 473–485.

Rogers A, Medlyn BE, Dukes JS, Bonan G, von Caemmerer S, Dietze MC, Kattge J, Leakey ADB, Mercado LM, Niinemets Ü *et al.* 2017. A roadmap for improving the representation of photosynthesis in Earth system models. *New Phytologist* **213**: 22–42.

Sabot MEB, De Kauwe MG, Pitman AJ, Medlyn BE, Ellsworth DS, Martin-StPaul NK, Wu J, Choat B, Limousin J-M, Mitchell PJ *et al.* 2022. One stomatal model to rule them all? Toward improved representation of carbon and water exchange in global models. *Journal of Advances in Modeling Earth Systems* **14**: e2021MS002761.

Sander R. 2023. Compilation of Henry's law constants (version 5.0.0) for water as solvent. *Atmospheric Chemistry and Physics* **23**: 10901–12440.

Sharkey TD, Bernacchi CJ, Farquhar GD, Singsaas EL. 2007. Fitting photosynthetic carbon dioxide response curves for C_3 leaves. *Plant, Cell & Environment* **30**: 1035–1040.

Slot M, Nardwattanawong T, Hernández GG, Bueno A, Riederer M, Winter K. 2021. Large differences in leaf cuticle conductance and its temperature response among 24 tropical tree species from across a rainfall gradient. *New Phytologist* **232**: 1618–1631.

Slot M, Rifai SW, Eze CE, Winter K. 2024. The stomatal response to vapor pressure deficit drives the apparent temperature response of photosynthesis in tropical forests. *New Phytologist* **244**: 1238–1249.

Smith NG, Keenan TF. 2020. Mechanisms underlying leaf photosynthetic acclimation to warming and elevated CO_2 as inferred from least-cost optimality theory. *Global Change Biology* **26**: 5202–5216.

Stefanski A, Butler EE, Bermudez R, Montgomery RA, Reich PB. 2023. Stomatal behaviour moderates the water cost of CO_2 acquisition for 21 boreal and temperate species under experimental climate change. *Plant, Cell & Environment* **46**: 3102–3119.

Takahashi Y, Joo H, Pankasem N, Hsu P-K, Schroeder JI. 2025. Stomatal CO_2 sensing in plants: control of gas exchange and interactions with environmental stimuli. *Plant and Cell Physiology* **66**: 1259–1273.

Urban J, Ingwers MW, McGuire MA, Teskey RO. 2017. Increase in leaf temperature opens stomata and decouples net photosynthesis from stomatal conductance in *Pinus taeda* and *Populus deltoides* × *nigra*. *Journal of Experimental Botany* **68**: 1757–1767.

Vialet-Chabrand S, Matthews JSA, Lawson T. 2021. Light, power, action! Interaction of respiratory energy- and blue light-induced stomatal movements. *New Phytologist* **231**: 2231–2246.

Wong SC, Canny MJ, Holloway-Phillips M, Stuart-Williams H, Cernusak LA, Márquez DA, Farquhar GD. 2022. Humidity gradients in the air spaces of leaves. *Nature Plants* **8**: 971–978.

Wood SN. 2017. *Generalized additive models: an introduction with R.* New York, NY, USA: Chapman and Hall/CRC.

Xu Z, Jiang Y, Jia B, Zhou G. 2016. Elevated-CO_2 response of stomata and its dependence on environmental factors. *Frontiers in Plant Science* **7**: 7–2016.

Zich FA, Hyland BPM, Whiffin T, Kerrigan RA. 2020. *Australian tropical rainforest plants edition 8.* Cairns: Australian Tropical Herbarium.

Supporting Information

Additional Supporting Information may be found online in the Supporting Information section at the end of the article.

Fig. S1 Temperature dependence of biophysical parameters underlying Medlyn *et al.* (2011) model parameter g_1.

Fig. S2 Images of study species used in this study.

Fig. S3 Diel pattern of environmental conditions within growth chambers across the experimental growing period.

Fig. S4 Comparison between leaf temperature (T_L) and vapour pressure deficit of the leaf (VPD_L) during gas-exchange measurements.

Fig. S5 Comparison of g_1 estimates made using regression-based estimate and the inversion method.

Fig. S6 Simulation of leaf-level gas exchange using *Photosyn* function in the R-package *Plantecophys* (Duursma, 2015), assuming either constant g_1 or temperature-sensitive g_1.

Fig. S7 Simulation of leaf-level gas exchange using *Photosyn* function in the R-package *Plantecophys* (Duursma, 2015), assuming temperature-sensitive g_1 under either near-ambient control (420 ppm) or elevated (820 ppm) [CO_2].

Fig. S8 Simulation of leaf-level gas exchange using *Photosyn* function in the R-package *Plantecophys* (Duursma, 2015), assuming temperature-sensitive g_1 under either constant VPD_L (1.6 kPa) or with VPD_L increasing in line with T_L.

Fig. S9 Impact of temperature on leaf-level gas exchange in four temperate tree species, data from Diao *et al.* (2024).

Please note: Wiley is not responsible for the content or functionality of any Supporting Information supplied by the authors. Any queries (other than missing material) should be directed to the *New Phytologist* Central Office.